INTAKE FLOW INVESTIGATION AT RUN-OF-RIVER POWER PLANT FLUHMÜHLE BY MEANS OF PHYSICAL MODELLING AND STEREOSCOPIC PIV MEASURING

Petr Lichtneger[1], Jürgen Stamm[2], Detlef Aigner[2] & Ulf Helbig[2]

[1]Institute for Hydromechanics, Karlsruhe Institute of Technology, Germany, Kaiserstr. 12, 76131 Karlsruhe
[2]Institute of Hydraulic Engineering and Technical Hydromechanics, Technische Universität Dresden, Germany, 01062 Dresden
E-mail: mail@iwd.tu-dresden.de

Abstract

The paper gives an overview of experiments which were done to investigate the intake flow on the Hydro Power Plant Fluhmühle. The project's aim was to model the flow physically and to simulate various flow conditions to evaluate their influence on the turbine operation with respect to the efficiency and the intake head losses. The free surface vortex occurring on the intakes was assumed to be the main problem. On the model stereoscopic particle image velocimetry was applied to get better insight into the flow structure inside the turbine intake. It has been shown, that the swirl flow with coherent vortices produces local extremes of both radial and axial velocity components in the intake which propagate deeper into the turbine passage. The damping effect of the trash rack onto the vortex strength was also demonstrated as well as the influence of the adjacent turbines.

Introduction

The submersed run-of-river Hydro Power Plant (HPP) Fluhmühle, constructed as 'Arno Fischer' type, equipped with four axial STRAFLO-turbines (with inclined axes of 27° and circumferential generators) was built on the Iller River (Bavaria) in 1944. Nowadays the plant is being operated in a heaving regime (German term 'Schwellbetrieb', s. Mosonyi, 1987). The plant possesses an installed capacity of 5.2 MW by the discharge of 100 cubic meters and the gross head is approximately 7.7 meters.

Under the current conditions swirling phenomena can be observed at the intakes. They are supposed to be the cause of operating problems at trash-rack and the turbine (trash-rack bar failures, increased cavitation at the runner) especially at the land side turbine. This one is exposed to an oblique approach flow due to the river bed formed by gravel-silt sediments. They have been accumulated during past flood events and have steep inclines close by the intake section equipped with trash rack and the cleaning machine. Consequently, the geometric boundary condition is strongly unsymmetrical, as shown in Figure 1. Furthermore, the flow boundary conditions, i.e. the flow rate and the combined operation with adjacent turbines and/or spillways, also affect the vortex characteristics – strength, location and orientation. The scale reduced physical FROUDE law model of the HPP Fluhmühle was designed and built at the length scale M_L = 20 in the Hubert-Engels-Laboratory of the Technische Universität Dresden.

Figure 1: A photograph with the HPP model structure; there are 4 intakes on the left bottom, 2 outlets on the right bottom and 4 flap gates on the top part of the plant.

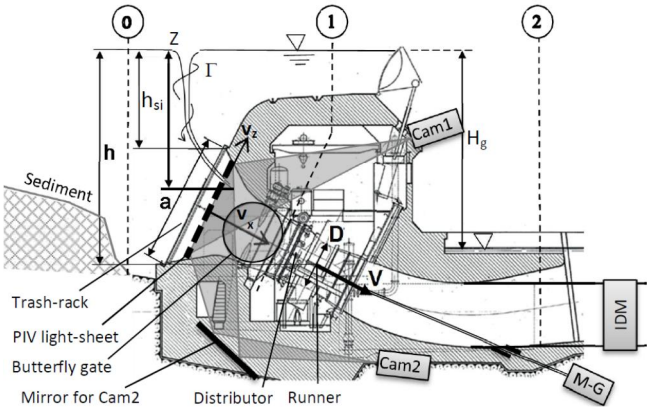

Figure 2: Longitudinal section of HPP Fluhmühle illustrating main parameters and the model equipment.

Intake vortex

An obliquely approaching flow is typical for intakes which are situated aside from the main stream, and it is one of the reasons which may induce the formation of intake vortex. Furthermore, free surface vortices are formed at intakes with low submergence depth, e.g. Knauss, 1987. A critical submergence depth, h_{cr}, needed for the vortex-free intakes can be preliminary assessed according to e.g. Gordon as recommended in Giesecke & Mosonyi, 2009:

$$h_{cr} = C \cdot V \cdot \sqrt{\frac{D}{g}} \quad [m] \tag{1}$$

In equation (1) is defined C = 2.3, or C = 1.7 for unsymmetrical and symmetrical intakes respectively, V is the bulk velocity and D is the diameter of the reference intake pipe.

$$\Gamma = \oint_L \boldsymbol{V} \cdot d\boldsymbol{l} = \iint_A \boldsymbol{\omega} \cdot d\boldsymbol{n} \quad [m^2/s] \tag{2}$$

The 'strength' of a vortex can be quantified by circulation *(Γ)*, see equation (2), where $\boldsymbol{V}$ is the velocity vector and $d\boldsymbol{l}$ is the line element of the closed loop L and where $\boldsymbol{\omega}$ is the vorticity vector and $d\boldsymbol{n}$ is the unit vector normal to the enclosed surface A, see e.g. Acheson, 1990. The reduction of circulation of the intake vortex or its vorticity respectively is the main task to ensure uniform, non-swirling flow conditions (keeping balanced turbine loading, low hydraulic losses, higher efficiency) and to avoid air introduction into the flow (avoiding vibration and cavitation). It is not easy to predict the circulation and the critical submergence depth, because the individual conditions are to be taken into account. Main parameters on which the circulation is dependent are given in equation (3).

$$\Gamma = f(Fr_{si}, \Pi, \Psi, Re, We) \tag{3}$$

The FROUDE number of submerged intake (Fr_{si}) is determined by equation (4) where h_{si} is the submergence depth. Modifying equation (2) a critical FROUDE number can be found for a given submergence, see equation (5).

$$Fr_{si} = \frac{V}{\sqrt{g \cdot h_{si}}} \quad [-] \tag{4}$$

$$(Fr_{si})_{cr} = \frac{1}{C} \cdot \sqrt{\frac{h_{si}}{D}} \quad [-] \tag{5}$$

Unfortunately, the definition of submergence depth, h_{si}, is ambiguous, because it differs depending on the author and type of investigated geometry. At HPP Fluhmühle Fr_{si} = 1.31 (for Q = 30 m^3/s) which is higher as $(Fr_{si})_{cr}$ = 0.63. So there is a good presumption of the vortex occurrence regardless of the bed topography. But using the submergence depth of the reference section (runner) or the velocity in reference to the wide intake section the submergence would be sufficient in relation to equation (1). Π in equation (3) covers in addition to the coefficient C other geometry features like the intake form (intake size a, diameter D etc.), the basin bed topography (incl. sediment depositions) as well as all 'anti-vortex' devices.

Ψ in eq. (3) covers other flow features, i.e. parameters of the approach flow, which may be influenced by e.g. operating adjacent turbines and/or spillways.

Scaling consistency

The REYNOLDS number, *Re*, and the WEBER number (*We*) cannot be preserved on a FROUDE law scaled model with the air-water interface. But there are some common criteria under which the internal friction and surface tension can be neglected by modelling of swirling flows and vortex formation, as summarised e.g. in Novak, Guinot, Jeffrey, & Reeve, 2010. Nevertheless the form of the vortex and air entrainment on a scale reduced model was more similar to that of a prototype if the circulation could be increased. In Zuikov, 2010, it was illustrated that the vortex form, particularly the vortex core depth *(Z)* depends besides the FROUDE number on the turbulent analogy of the REYNOLDS number, (Re_t) even if *Re* and *We* are considered to be negligible. Consequently, the model velocity with respect to the FROUDE law (V_{Fr}) should additionally be modified by factor $M_L^{3/14}$, see equation (6), to obtain the velocity *(V)* at which the vortex funnel depth on the model corresponds to the linear length scale factor (M_L), or the vortex funnel depth obtained by the FROUDE law model should be converted to the prototype by factor $M_L^{3/2}$, see equation (7).

$$\frac{V}{V_{Fr}} = M_L^{3/14} \quad [-] \tag{6}$$

$$\frac{Z_{Prototype}}{Z_{Model}} = M_L^{3/2} \quad [-] \tag{7}$$

A strong vortex has been observed on the HPP Fluhmühle as shown in Figure 3.

Figure 3: Photographs showing a good match of the intake free surface vortex on the HPP Fluhmühle (left) and of its model (right) with the land side turbine in operation only.

Thus for the length scale of 20 the velocities on the physical model should be 1.9-times higher as with respect to the FROUDE law according to the equation (6), which would require increasing the turbine discharge appropriately. According to the equation (7), the vortex dimple would be 90-times smaller on the model than observed on site, and not just only 20-times as with respect to the FROUDE law. Both represent a problem for the feasibility of correct scaled physical modelling because the intake vortex circulation and the appropriate flow vorticity

field, as referred in equation (2), cannot be modelled quantitative identically with the prototype.

Hydraulic model experiments

The hydraulic model (M_L = 20, *Fr = idem*) encompassed the river bed region starting approximately 150 m upstream the HPP with weir gates, bottom outlets, piers and 4 intakes including butterfly turbine gates (Figure 1). To ensure the similarity of upstream bed topography and approaching velocities at the model inlet on-site ADCP measurements were carried out (Stamm, Aigner, & Lichtneger, 2011). The intake flow at the land side turbine, T1, was to be investigated primarily regarding its influence onto the turbine efficiency and the trash rack losses. The parameters in equation (3) were held constantly except the flow parameter *(Ψ)* which was modified due to combining the turbines in operation, and the form parameter *(Π)* alternating the tests with and without trash-rack (see Table 1).

Table 1: Tested turbine combinations at $F_{r,si}$ = 1.1 (Q = 25 m^3/s); TR – trash-rack, CW – clockwise, CCW – counter clockwise, the vortex strength type ref. to Knauss, 1987, entrance quadrants (RU, LD) ref. to Figure 7.

Identifier (A, …, H)	Discharge (m^3/s)				Vortex observation at T1 without TR
TR = 1/0 (with or w/o)	T1	T2	T3	T4	Direction; Strength type; Entrance
A1 / A0	25	0	0	0	CW, 5-6, RU
B1 / B0	25	25	0	0	CW, 2-6, RU
C1 / C0	25	0	25	0	CCW, 1-3, LD
D1 / D0	25	0	0	25	CCW, 1-4, LD
E1 / E0	25	25	25	0	CCW, 1~3, LD
F1 / F0	25	0	25	25	CCW, 2~4, LD
G1 / G0	25	25	0	25	CCW, 1-4, LD
H1 / H0	25	25	25	25	CCW, 2-4, LD

The land side intake (T1) was equipped with a geometrically similar model turbine. Both, intake and turbine were mostly made from acrylic glass to allow flow observations and optical measurements. The other 3 intakes (T2-T4) were modelled without turbine equipment except the butterfly gates and the discharge was each controlled with triangular spillways. The measurements of the static water column levels in sections '0', '1' and '2' (Figure 2) installed on T1 and T3 allowed to estimate turbine heads and intake head losses.

Turbine

All functional turbine parts like the runner (propeller with 5 blades), the guide vanes (12) and the stay vanes (4 ahead, 3 in the tail) were modelled on the land side turbine T1 in scale. Due to the strong model size reduction the limit conditions for correct hydraulic modelling of rotational hydro machines like the minimal Reynolds number (4 Mio.), the minimal head (3 m) or the minimal turbine diameter (0.3 m) could not be satisfied as proposed in IEC 60193, 1999. That is why the friction losses increase and thus the model turbine efficiency drops down rapidly. Furthermore, there were mechanical losses from a small dc motor-generator (M-G), which was installed on the model shaft to control the turbine speed, and the bearing losses rising with the hydrodynamic axial force on the model. The total mechanical loss, roughly set as $P_{Lm} \approx n^2$, was inadequate high to the disposal scaled hydraulic power. So the motor-generator had to be run in the motor mode to keep the turbine at model speed.

Table 2: Turbine characteristics, T1; for the stated parameters see e.g. Mosonyi, 1987.

Parameter	Prototype	Model
Runner diameter (D)	2.1 m	0.1 m
Tested discharge (Q)	25 m^3/s (30)	0.014 m^3/s (0.017)
Speed (n)	214.3 rpm	957 rpm
Net head (H)	app. 6.85 m	0.25-0.4 m *)
Guide vane opening	70 % ⇔ 55° (82 % ⇔ 64°)	
Unit speed (n_{11})	170 rpm	
Unit discharge (Q_{11})	2.2 (2.6) m^3/s	
Specific speed (n_s ; n_q)	≅ 870 (910) ; 253 (277) rpm	
$Re = VD/\nu$	18.3 Mio.	0.2 Mio.

*) depending on the current suction head of the model outlet pipe

The needed power to accelerate the runner in motor mode (P_M), was used to calculate the relative efficiency (η_{rel}) of the model turbine, see equation (8). The M-G efficiency was simply supposed to be constant or monotone in the tested range of speed and power.

$$\eta_{rel,motor-mode} = \frac{P_{Lm}}{P_h + P_M} \cdot 100 \quad [\%] \tag{8}$$

The hydraulic power (P_h) was calculated from the net head (H) between sections '2' and '3' (see Figure 2), and the turbine discharge (Q) which was measured with an inductive flow meter on the outlet pipe of the turbine T1 and controlled by a slider. The draft tube was not modelled assuming that it has no influence on the intake flow. Hence, the net head on the model was approximately 80 cm lower compared to that on the prototype. This and imperfections in the geometrical similarity also caused additional deviations from the prototype efficiency. Furthermore, the missing draft head was sometimes reached due to the suction of the outlet pipe downwards the slider. Thus there was an unstable head on the hydraulic model causing difficulties in repeatability (keeping the position in efficiency hill diagram – n_{11}-q_{11}), which was to be considered by evaluating of measurements. An array of efficiency measurements depending on speed as well as of

the efficiency results from the comparative measurements with parameters given in Table 1are plotted in Figure 4.

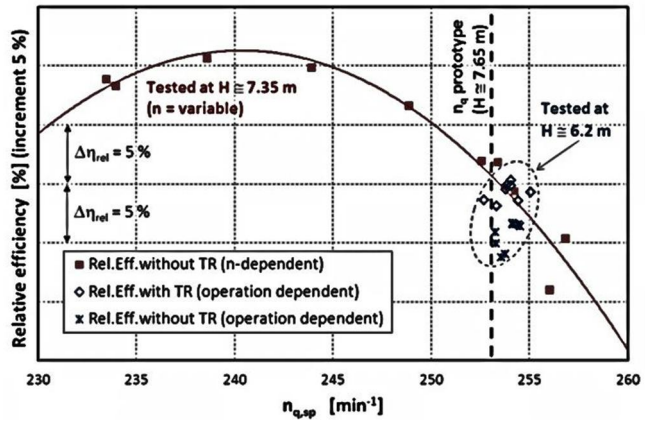

Figure 4: Relative efficiency chart converted to the specified net head H_{sp} = 7.65 *m*; $n_{q,sp} = n \cdot Q^{0.5} H_{sp}^{-0.75}$.

Based on the comparative measurements it could be preliminary estimated that, first, the turbine efficiency with trash rack was higher than without it (by app. 1 % taking into account the efficiency slope on n_q), second, the turbine combination 'A' (Table 1) showed mostly the worst efficiency, third, the turbine combination 'E' showed mostly the best efficiency. At the combination 'A' the strongest and 'E' the weakest vortices were observed on T1.

Figure 5: Intake vortex at turbine combination 'B0'; the air core entered the T1 and T2 alternately.

The particular turbine combinations resulted in a change of the strength, direction and localisation of the intake vortex (see Table 1). Indeed, different free surface vortices were occurring not only at intake T1 but also at other intakes simultaneously. For example in case 'B' the intake vortex entered even both the intake T1 and T2 alternately in time as shown in Figure 5.

Trash rack

The trash rack was also modelled according to FROUDE law expecting the self-similarity relevance. Its main parameters are given in Table 3. The trash rack showed a significant damping effect on the free surface vortices at the hydraulic model. For better similarity of the vortex strength with nature it was necessary to remove the trash rack to allow the intake vortex strength growing. That is why the vortex vs. trash-rack interaction was weaker on the scale reduced model than that in nature, and hence the total intake head loss was significant higher at the intakes on prototype compared to model tests as shown in Figure 6.

Table 3: Prototype and model trash-rack parameters.

Parameter	Prototype	Model
Bar thickness (t)	10 mm	0.5 mm
Bar depth (d)	100 mm	5 mm
Clear spacing (b)	50 mm	2.5 mm
Trash rack area (A_r)	28.6 m^2	0.072 m^2
Trash rack declination (α)	63°	
$Re_r = V_r \cdot t/\nu$	10 000	100

The intake head loss was measured between sections '0' and '1' (see Figure 2) at the model as well as at the prototype. Thus the trash-rack losses and also the losses due to the flow acceleration and due to the butterfly gate were included. The net head loss of just the model trash-rack itself was estimated to about 10 cm.

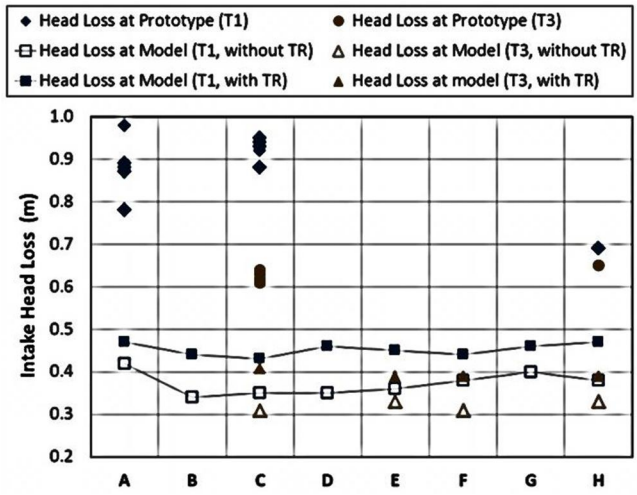

Figure 6: Comparison of intake head losses of prototype and model (intakes T1 and T3 at several operational combinations according to Table 1).

The difference between model and prototype was about 40 cm of water column at T1 and about 20 cm at T3. There are two main sources which could cause high additional head losses on the prototype: first, the blockage of the trash-rack with floating debris, second, the in nature stronger swirling flow itself. Using a novel formula by Meusburger, 2002, for the trash-rack head loss which also takes into account the debris blockage ratio (German term: 'Verlegung'), the measured results correspond to a blockage of minimal 20 % of the intake trash-rack area. More probably both the debris and the swirl had caused higher losses in nature. Regarding the equations (6) and (7) the swirling flow could not be modelled in scale correctly, which led to underestimating the intake losses (with as well as without the trash-rack) of the model. Unfortunately, there are no guidelines in literature for the quantification of the trash-rack head loss resulting from the swirling flow.

Stereoscopic PIV

The stereoscopic Particle Image Velocimetry (stereo-PIV) was implemented on the hydraulic model to capture the velocity fields (3-component vectors in a plane) inside the intake behind the trash-rack section of the land side turbine (Lichtneger & Aigner, 2011).

Table 4: Main parameters of the used stereo-PIV system.

Software	TSI Insight3G, Tecplot, Matlab
Laser	Nd:YAG New Wave Solo Laser 532 nm, 2x100 mJ, rep. rate 15 Hz
Cameras	2 x Power-View Plus 2MP Camera 1600x1200 Pixel, Nikon 28mm Lenses
Synchronizer	TSI Laser Pulse Synchronizer 610034
Seeding	VESTOSINT Polyamide 12 d_{50} = 100 µm, ρ = 1060 kg/m^3
Processing	Ensemble FFT, Rec. Nyquist Grid IA $32^2/16^2$, h. filling 3^2, smoothing 5^2 px.

The ensemble FFT cross correlation, the holes filling and smoothing methods allowed compensating for a lack in homogeneity of the seeding. Thus no turbulence statistics could be analysed. The resulting velocity fields represented an about 6 second average of the quasi stationary flow, which caused variable accuracy depending on the seeding density and the vortex fluctuation. Because both PIV cameras were partly blanked out by the butterfly gate there are gaps in the resulting contours. Also the contour margins could not be evaluated because of high image refraction due to the wall curvature of the intake cone.

The axial and cross-stream components of velocity, equations (9) and (10), and the axial component of vorticity, equation (11), were evaluated and normalised by the bulk velocity of the measurement plane and by the turbine speed respectively. The results from the configuration with the measurement plane placed in the cross-section 150 cm behind the trash-rack (see Figure 2) are introduced here for two flow conditions, namely ‘A’ and ‘H’ as defined in Table 1. They differ from each another in the vortex position and sense of rotation as shown in Figure 7.

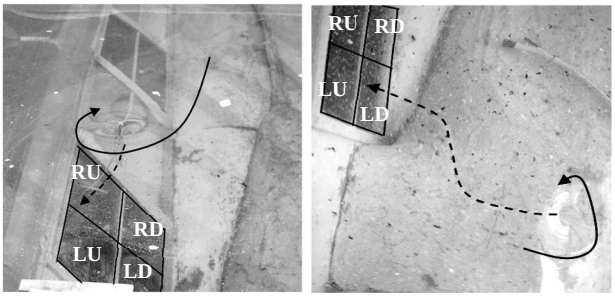

Figure 7: Vortex formation at T1 under flow conditions ‘A0’ (left) and ‘H0’ (right). The entrance quadrants are denoted (RU – right up, LD – left down, etc.).

$$V_{ax} = \frac{V_x}{V_{bulk}} \quad [-] \tag{9}$$

$$V_{cross} = \frac{\sqrt{V_y^2 + V_z^2}}{V_{bulk}} \quad [-] \tag{10}$$

$$\omega_{ax} = \frac{60 \cdot \omega_x}{n} \quad [-] \tag{11}$$

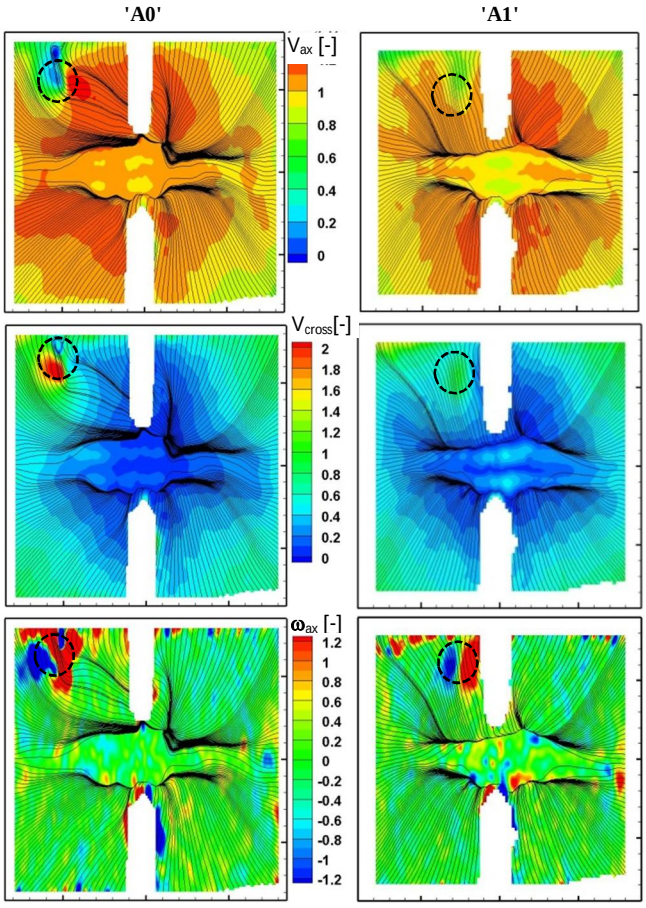

Figure 8: Velocity and vorticity fields [ref. to equations (9, 10 & 11) above] with streamlines from the stereo-PIV at intake T1 under flow condition ‘A0’ (left) and ‘A1’ (right) as defined in Table 1; plotted in the upstream view. The circles indicate the vortex core position approximately.

Under the turbine combination ‘A0’ the intake vortex core reached to the measurement profile and blocked the flow field in the right upper corner totally (downstream view), which produced local extreme values and gradients of both the axial and cross-stream velocity components, as plotted in Figure 8 on the left. Whereas in the case with the trash-rack, see Figure 8 on the right, the velocity gradients became much lower due to the trash-rack damping effect on the vortex; although the vorticity remained rather unchanged quantitatively. Typically two opposite vorticity peaks were evaluated side-by-side.

Under the turbine combination ‘H0’ (Figure 9) the relatively weak vortex decelerated the flow a little in the

left bottom corner. Just only one significant peak could be estimated in the vortex field. Nevertheless, all discussed cases show deviations from an optimal axial symmetrical flow distribution which was approximated best by turbine combination ‘E1’ (see the Figure 9 on the right down).

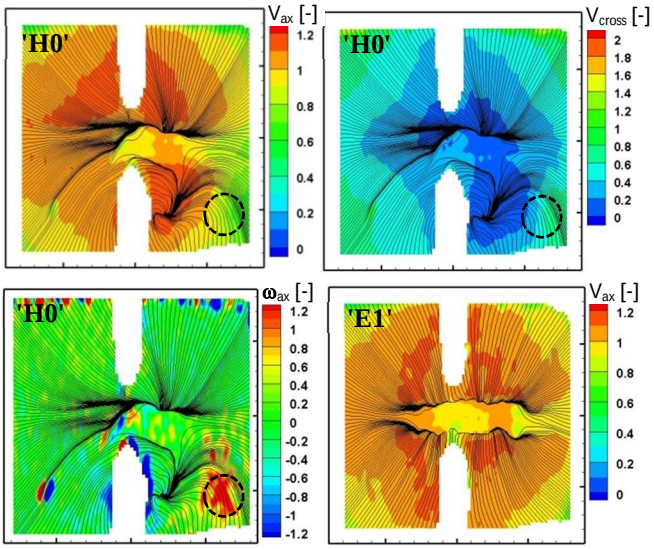

Figure 9: Velocity and vorticity fields with streamlines at intake T1 and flow condition ‘H0’ (left and up right) and ‘E1’ (right down); plotted in the upstream view.

Comparing the cases ‘A0’ and ‘A1’ gives an idea about the work of the trash-rack, so to say an ‘anti-vortex’ device, by steadying and equalising the flow. Especially if interacting with the air core the trash-rack failure becomes much more probable because of the high velocity gradients fluctuating in time.

Conclusion

It was attempted to model the intake flow influence on the turbine efficiency directly. The high mechanical losses of the model turbine, the motor based turbine power measurement and the unstable tailrace water have caused high scatter of efficiency data, therefore the results are to be understood as preliminary. A direct torsion measurement and a stabilising of the tailrace water elevation would probably help to get the desired improvement. The intermittency of the vortex strength fluctuation also affected the measurement repeatability. The latter was a problem for the PIV measurements, which were evaluated as an ensemble average over a short time period because of seeding difficulties and the limited image storage capacity. Though, various velocity and vorticity fields were measured behind the trash-rack section for different approaching flow conditions by the stereo-PIV. The flow in front of the turbine differed from the ideal boundary condition as usually assumed designing a turbine profile. Some typical examples are presented here showing the vortex influence on the flow distribution and the damping effect of the trash-rack. In cases with a fully developed vortex air core, the vortex path through the turbine could also be studied at the transparent turbine model.

It is supposed, that the strength of the modelled surface vortices do not correspond to the prototype in scale as discussed in the introduction, which would help to explain the disagreement of model and prototype head loss measurements at the intakes. On prototype, the stronger vortex could cause a stronger redistribution of the mean flow with higher extremes and gradients in the cross-section. Thus the relation of the real kinetic energy in the cross-section and the energy calculated from the mean velocity would be higher in nature than at the model. Verifying this hypothesis and furthermore, the quantification of the swirl interaction with the trash-rack and its effect on the turbine efficiency, is generally still to be investigated yet.

Acknowledgements: This research was supported by a Marie Curie Intra European Fellowship within the 7th European Framework Programme and by the plant operator Bayerische Elektrizitätswerke (BEW).

References

IEC 60193. (1999). Hydraulic turbines, storage pumps and pump-turbines - Model acceptance tests.

Acheson, D. (1990). Elementary Fluid Dynamics. Oxford: Clarendon Press.

Aigner, D., Lichtneger, P., & Martin, H. (2010). Use of the Stereo PIV System for Capture of Intake flow Patterns on a Physical Model of a Bay-type Run-of-river Power plant. Fachtagung "Lasermethoden in der Strömungsmesstechnik". Cottbus: GALA e.V.

Giesecke, J., & Mosonyi, E. (2009). Wasserkraftanlagen. Springer-Verlag.

Knauss, J. (1987). Swirling flow problems at intakes. Rotterdam: Balkema.

Lichtneger, P. (2011). Untersuchungen zur Optimierung der Einlaufströmung an Niederdruckwasserkraftanlagen. 34. Dresdner Wasserbaukolloquium 2011: Wasserkraft – mehr Wirkungsgrad + mehr Ökologie = mehr Zukunft. Dresden: Technische Universität Dresden.

Lichtneger, P., & Aigner, D. (2011). Use of the Stereo PIV System for Determination of the Intake Flow Patterns on a Physical Model of a Run-of-river Power Plant with Tubular Turbines. Fachtagung "Lasermethoden in der Strömungsmesstechnik". Ilmenau: GALA e.V.

Meusburger, H. (2002). Energieverluste an Einlaufrechen von Flusskraftwerken. (Vols. Mitteilungen. Heft 179 der Versuchsanstalt für Wasserbau, Hydrologie und Glaziologie der ETH Zürich). Zürich: ETH Zürich.

Mosonyi, E. (1987). Low-Head Power Plants. Budapest: Akademiai Kiado.

Novak, P., Guinot, V., Jeffrey, A., & Reeve, D. E. (2010). Hydraulic Modelling - an Introduction. London: Spon Press.

Stamm, J., Aigner, D., & Lichtneger, P. (2011). Flusskraftwerk Fluhmühle: Auswerung Vor-Ort-Messungen. Dresden: Institut für Wasserbau und Technische Hydromechanik, Technische Universität Dresden.

Zuikov, A. L. (2010). Peculiarities of physical modeling of surface vortex funnels. Power Technology and Engineering, pp. 15-19.